Characterizing the Sensitivity of 40 GHz TES Bolometers for BICEP Array

C. Zhang[1] · **P. A. R. Ade**[2] · **Z. Ahmed**[3,4] ·
M. Amiri[5] · **D. Barkats**[6] · **R. Basu Thakur**[1] ·
C. A. Bischoff[7] · **J. J. Bock**[1,8] · **H. Boenish**[6] ·
E. Bullock[9] · **V. Buza**[6] · **J. Cheshire**[9] ·
J. Connors[6] · **J. Cornelison**[6] · **M. Crumrine**[9] ·
A. Cukierman[4] · **M. Dierickx**[6] · **L. Duband**[10] ·
S. Fatigoni[5] · **J. P. Filippini**[11,12] · **G. Hall**[9] ·
M. Halpern[5] · **S. Harrison**[6] · **S. Henderson**[3,4] ·
S. R. Hildebrandt[8] · **G. C. Hilton**[13] · **H. Hui**[1] ·
K. D. Irwin[3,4] · **J. Kang**[4] · **K. S. Karkare**[6,14] ·
E. Karpel[4] · **S. Kefeli**[1] · **J. M. Kovac**[6] ·
C. L. Kuo[3,4] · **K. Lau**[9] · **K. G. Megerian**[8] ·
L. Moncelsi[1] · **T. Namikawa**[15] · **H. T. Nguyen**[8] ·
R. O'Brient[8,1] · **S. Palladino**[7] · **N. Precup**[9] ·
T. Prouvé[10] · **C. Pryke**[9] · **B. Racine**[6] ·
C. D. Reintsema[13] · **S. Richter**[6] · **A. Schillaci**[1] ·
B. Schmitt[6] · **R. Schwarz**[6] · **C. D. Sheehy**[16] ·
A. Soliman[1] · **T. St. Germaine**[6] · **B. Steinbach**[1] ·
R. V. Sudiwala[2] · **K. L. Thompson**[3,4] · **C. Tucker**[2] ·
A. D. Turner[8] · **C. Umiltà**[7] · **A. G. Vieregg**[14] ·
A. Wandui[1] · **A. C. Weber**[8] · **D. V. Wiebe**[5] ·
J. Willmert[9] · **W. L. K. Wu**[14] · **E. Yang**[4] ·
K. W. Yoon[4] · **E. Young**[4] · **C. Yu**[4]

the date of receipt and acceptance should be inserted later

[1]Department of Physics, California Institute of Technology, Pasadena, California 91125, USA

[2]School of Physics and Astronomy, Cardiff University, Cardiff, CF24 3AA, United Kingdom

[3]Kavli Institute for Particle Astrophysics and Cosmology, SLAC National Accelerator Laboratory, 2575 Sand Hill Rd, Menlo Park, California 94025, USA

[4]Department of Physics, Stanford University, Stanford, California 94305, USA

[5]Department of Physics and Astronomy, University of British Columbia, Vancouver, British Columbia, V6T 1Z1, Canada

[6]Harvard-Smithsonian Center for Astrophysics, Cambridge, Massachusetts 02138, USA

[7]Department of Physics, University of Cincinnati, Cincinnati, Ohio 45221, USA

[8]Jet Propulsion Laboratory, Pasadena, California 91109, USA

[9]Minnesota Institute for Astrophysics, University of Minnesota, Minneapolis, 55455, USA

[10]Service des Basses Températures, Commissariat à lEnergie Atomique, 38054 Grenoble, France

[11]Department of Physics, University of Illinois at Urbana-Champaign, Urbana, Illinois 61801, USA

[12]Department of Astronomy, University of Illinois at Urbana-Champaign, Urbana, Illinois 61801, USA

[13]National Institute of Standards and Technology, Boulder, Colorado 80305, USA

[14]Kavli Institute for Cosmological Physics, University of Chicago, Chicago, IL 60637, USA

[15]Department of Applied Mathematics and Theoretical Physics, University of Cambridge, Wilberforce Road, Cambridge CB3 0WA, UK

arXiv:2002.05219v1 [astro-ph.IM] 12 Feb 2020

Abstract The BICEP/Keck (BK) experiment aims to detect the imprint of primordial gravitational waves in the Cosmic Microwave Background polarization, which would be direct evidence of the inflation theory. While the tensor-to-scalar ratio has been constrained to be $r_{0.05} < 0.06$ at 95% c.l., further improvements on this upper limit are hindered by polarized Galactic foreground emissions and removal of gravitational lensing polarization. The 30/40 GHz receiver of the BICEP Array (BA) will deploy at the end of 2019 and will constrain the synchrotron foreground with unprecedented accuracy within the BK sky patch. We will show the design of the 30/40 GHz detectors and test results summarizing its performance. The low optical and atmospheric loading at these frequencies requires our TES detectors to have low saturation power in order to be photon-noise dominated. To realize the low thermal conductivity required from a 250 mK base temperature, we developed new bolometer leg designs. We will present the relevant measured detector parameters: G, T_c, R_n, P_{sat}, and spectral bands, and noise spectra. We achieved a per bolometer NEP including all noise components of 2.07×10^{-17} W$/\sqrt{\text{Hz}}$, including an anticipated photon noise level 1.54×10^{-17} W$/\sqrt{\text{Hz}}$.

Keywords Cosmology, B-Mode polarization, Inflation, CMB, TES

1 Introduction

Inflation theory builds upon the Standard Cosmological Model to provide an explanation of the origin of structure in our universe. Many families of inflationary models predict the presence of primordial gravitational waves, which would leave imprints in the Cosmic Microwave Background (CMB) polarization during recombination. BICEP/Keck (BK) experiments are aiming to measure the degree-scale B-mode polarization pattern in the CMB, which could constrain the tensor-to-scalar ratio r and place limits on the energy scale and potential of Inflation.

The gravitational wave induced B-mode patterns are very faint- modern experiments constrain the tensor-scalar ratio to be $r_{0.05} < 0.06$ at 95% confidence level with $\sigma(r) = 0.02$ [1]. These experiments must also constrain and remove B-modes from lensing of E-modes by large scale structure and the polarized emission from galactic foregrounds such as dust and synchrotron. Galactic foregrounds have a different spectral signature than the CMB, which allows component separation with multi-frequency observations. Keck receivers operating at 220 and 270 GHz, added in 2015 and 2017 respectively, have provided the ability to constrain the dust foreground in our observing sky patch.

BICEP Array (BA) [2][3] is the new generation of BK experiments, which will observe through the atmospheric windows between 30 and 270 GHz with a total of four receivers. The first receiver will observe at 30 and 40 GHz to constrain the synchrotron foreground. The receiver is designed to resolve $35 < l < 300$ features in a 600 deg^2 sky patch. The focal plane of BA will include twelve 6-inch detector modules. Half of the first camera's focal plane modules will have 30 GHz detectors while the others will have 40 GHz detectors, providing total detector counts of 192 and 300 respectively. The detectors we are using in this first receiver at 30/40 GHz are Transition Edge Sensor (TES) bolometers coupled with polarization-sensitive coplanar slot antennas. In this paper we will mainly focus on the detector development of 30/40 GHz. The central engineering challenge for these low

[16]Physics Department, Brookhaven National Laboratory, Upton, NY 11973
E-mail: czzhang@caltech.edu

frequency detectors is realizing background-limited noise performance from a 250 mK base temperature, which requires a high degree of thermal isolation. See [5] for an overall update of first BA receiver and [6] for the detailed antenna design and beam characterization.

2 Antenna and Bolometer Design
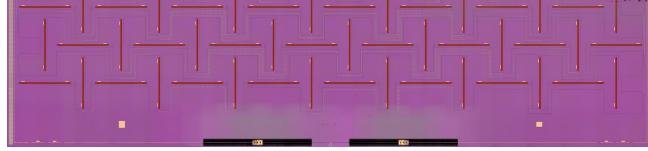
Fig. 1 Photo of the edge of a 40 GHz pixel, with bolometers and filters visible. The two orientations of slot antennas separately receive the two linear polarizations. The power from each set of slots is collected by the microstrip summing trees, passes through the band-pass filter on the lower corners of the photo, and thermalizes in the two TESs on the bottom. The two filters and bolometers separately receive the two linear polarizations.(color version online)

Fig. 2 Photo of a TES bolometer from a 40 GHz detector. The bolometer island is suspended from the thermal bath (the detector tile) by six ~ 1.4 mm-long legs, forming a weak thermal link. The thickness of the membrane is 1 μm. (color version online)

As shown in Figure. 1, the antenna coupled TESs used in BA 30/40 GHz are following the traditional design of the former BK experiments, operating at bath temperature T_{bath} about 250 mK, using two sets of slot antennas oriented in orthogonal directions to measure the polarized linear Stokes parameters. The size of the individual slots is much larger in 30/40 GHz than in the former higher frequency bands, and the 8×8 slots arrays result in pixel sizes of $\sim 25 \times 25$ mm^2 for 30 GHz and $\sim 20 \times 20$ mm^2 for 40 GHz. In each detector tile we have 4×4 and 5×5 imaging arrays of pixels for 30 and 40 GHz, respectively. The large pixel size and low detector count impose stringent uniformity and yield requirements across the wafer.

For each polarization, a microstrip summing tree is used to collect and coherently sum the power from all the antenna slots. The final microstrip line passes through a band-pass filter that defines the optical band of the camera, before depositing power on the detector island. Figure. 2 is a zoom-in photo of one of the 40 GHz bolometers. The gold meander on the detector island is an open-ended microstrip whose impedance is well matched to the superconducting transmission line. It terminates the end of the microstrip circuit, converts optical power into heat before the reflected EM wave get back out to the transmission microstrip.

The Niobium patterns on the gold meander as shown in the photo are designed to optimize the absorption of the optical power at 30 and 40 GHz. There are two TESs connected in series on each detector island- the Ti TES will be used in sky observation while the Al one is used in optical testing thanks to its higher saturation power P_{sat}. Detailed information of the detector island structure can be found in [4].

The detector island is suspended by 6 legs, forming the weak thermal link between the island and thermal bath with a thermal conductivity G. The length of the legs are chosen in order to meet the photon-noise dominant criteria while avoiding saturation during operation. The fabricated 40 GHz bolometers (shown in Figure. 2) have leg lengths targeting saturation powers 2.5 times of the expected optical loading. We define a safety factor SF as the ratio between saturation power and the optical loading. As a comparison, the leg length of 95 GHz bolometers used in BICEP3 was roughly half this length. The longer leg gives lower G, thereby suppressing the phonon noise to be subdominant to photon noise. The expected G is 14.5 pW/K (at 450 mK).

We explored further increasing sensitivity by suppressing the thermal bath temperature T_{bath}. The computed noise equivalent power (NEP) contributions from different noise components of 2 different bolometer designs are shown in Figure. 3. The left bar is the BA design, with $T_{bath} = 250$mK, giving a total NEP 3.98×10^{-17} W/$\sqrt{\text{Hz}}$. A design operating at $T_{bath} = 100$ mK is present at right. Both cases are assuming $SF = 2.5$. The lower bath temperature gives a NEP 12% lower, but the cost and complication of a more powerful dilution refrigerators required to achieve these lower temperatures is difficult for our team to justify for such marginal gains.
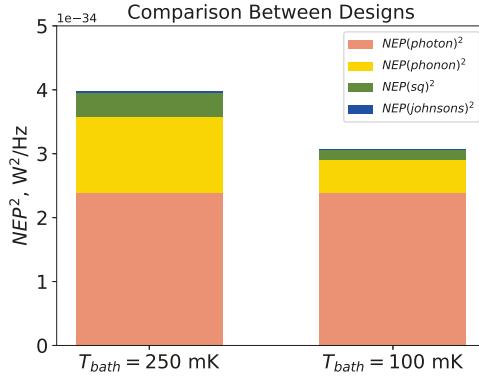

Fig. 3 NEP contributions of two different 40 GHz bolometer designs, both assuming SF=2.5. *Left* Bolometer design with $T_{bath} = 250$ mK. It is very close to the bolometer we are currently using for BA, requiring low G bolometer design as described in text. *Right* A design with $T_{bath} = 100$ mK. T_c and Operating impedance are also shifted down by 2.5 in this case. While the NEP benefits from a lower bath temperature by a factor of $\sqrt{3.07/3.98} = 0.88$, the expense and effort cannot be justified for this application when weighed against other needs.(color version online)

3 Measured Detector Parameters

We have fabricated and tested several 40 GHz detector tiles with the same antenna and filter design but different bolometer leg lengths, of which three have the desired bolometer properties (the design is shown in Figure 2). Spectra have been measured for the fabricated devices using a Fourier Transform Spectrometer (FTS). The average 40 GHz spectrum is shown in Figure.4, with band center at 41.5 GHz and ~28% bandwidth. For reference, we co-plot the typical atmospheric transmission at South Pole.
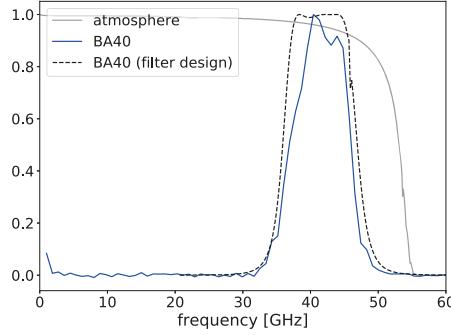
Fig. 4 Normalized detector spectra and South Pole atmospheric transmission. The *blue solid line* shows the averaged 40 GHz spectrum, with band center at 41.5 GHz and 28% band width. The *black dash line* shows the designed 40 GHz bandpass filter. The *black solid line* shows typical atmospheric transmission at the South Pole.(color version online)

The optical response of the detectors has been measured using two aperture-filling black body sources at room (300 K) and liquid nitrogen (77 K) temperatures. These results together with the measured spectra provide an estimate of the end-to-end optical efficiency-roughly 31%. The expected total optical loading is calculated within our 30/40 GHz band pass. We got 1.0 pW for 40 GHz, and 0.5 pW for 30 GHz, including loading from CMB and atmosphere, as well as reflective and absorptive losses in the test-bed filter stack and window. The in-band loading from atmosphere has an averaged temperature of 220 K with absorptivity of 0.06.

The left panel of Figure.5 shows the measured saturation for one 40 GHz tile operated at ~275 mK, showing a median value of 2.5 pW with most of the detectors scattered between 1.5 and 3 pW. This result matches our design target of P_{sat} ~2.5 times the total optical loading. We have also measured the P_{sat} at a series of T_{bath} to fit the result using $P_{sat} = G_c(T_c^{\beta+1} - T_{bath}^{\beta+1})/T_c^{\beta}(\beta + 1)$. G_c is the thermal conductivity between detector island and thermal bath measured at the TES transition temperature T_c, which is ~500 mK for our Ti TESs. The temperature index β is typically 2 for our bolometer design. A histogram of G scaled to 450 mK with $G_{450} = G_c(450/T_c)^{\beta}$ is shown in the right panel of Figure. 5, with a median value of 15.9 pW/K.

Figure. 6 shows a wafer map of T_c and the normal resistance of the titanium TESs on one 40 GHz tile, illustrating spatial achieved uniformity. Such studies are important because we recently switched from fabricating on 100 mm diameter tiles to 150 mm diameter tiles, and uniformity is not guaranteed over these larger surfaces. Non-uniformity in R_n exists as
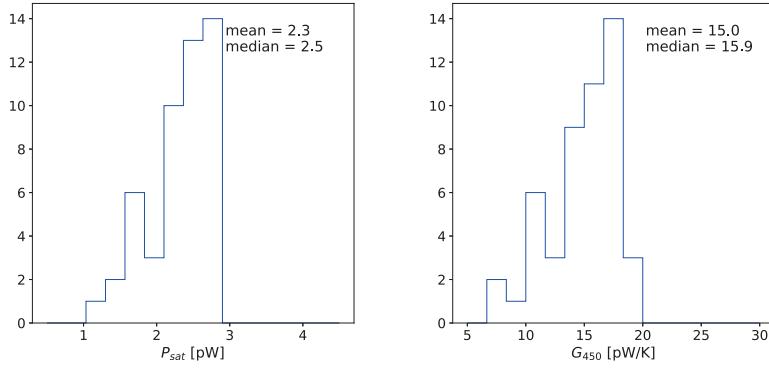
Fig. 5 Histograms of P_{sat} and G_{450} of one 40 GHz tiles. *Left, P_{sat}*, measured with an operation bath temperature of 275 mK, has a median of 2.5 pW with most of the detectors between 1.5 to 3 pW. *Right,* the bolometer island thermal conductivity at 450 mK G_{450} has a median of 15.9 pW/K. (color version online)
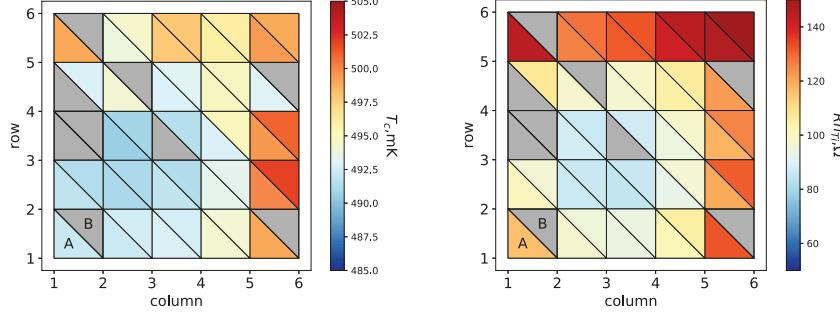

Fig. 6 The tile map of T_c and Rn_{Ti}. The triangles in each square represent the two bolometers for the orthogonal polarization within each pixel. Grey halves represent inoperational bolometers. T_c is uniform and well controlled to be ~500 mK. (color version online)

shown in left panel of Figure. 6, which may add difficulty to find a common bias in columns of our SQUID-based time division multiplexing readout. The thickness of Ti film has been measured over the 150 mm wafer. The variance between edge and center is about 15% of the average value, which is not enough to explain the large scattering of R_n. We think the variance could be caused by some contact problems that exist within or between layers. Efforts have been made in modifying fabrication process to fix this problem in the future. For the upcoming season, we took noise measurements at multiple bias points and confirmed the fabricated devices can work stably with photon noise dominant in a range of common bias points with operating resistance between 40 and 75 mΩ.

4 Background Noise Measurements and Expected Sensitivity

We fabricate some detectors on our tiles without antennas to function as dark bolometers and provide a baseline for noise performance. Figure. 7 shows the noise spectrum of one such detector, but with the tile module covered to further limit optical stimulation. The grey and purple lines represent the dark noise spectra of an individual detector and of the pair-difference time stream between two detectors in the same pixel. The estimated photon noise level according to expected optical loading at 40 GHz is given in light blue. Adding the measured noise at 0.1 Hz with estimated photon noise of 1.54×10^{-17} W/$\sqrt{\text{Hz}}$, we expect a total NEP 2.07×10^{-17} W/$\sqrt{\text{Hz}}$. Given that the science band is between 0.05 and 1 Hz in BK with a telescope scan rate of 2.8 deg/s, this plot is a preliminary validation of our photon-noise dominated design.
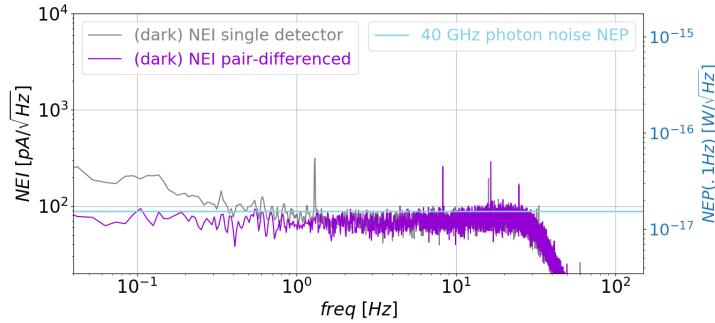
Fig. 7 The current noise spectrum of a 40 GHz dark detector measured in a covered configuration. The grey line is the spectrum of an individual bolometer and the purple line is the difference spectrum of between 2 detectors of polarization A and B in same pixel, divided by $\sqrt{2}$ to aid comparison to the single detector spectrum. The suppressed low frequency noise demonstrates that the 1/f effects are common mode and thus removable. The light blue line shows the expected photon noise level of 1.54×10^{-17} W/$\sqrt{\text{Hz}}$. The estimated total NEP including the measured background noise and photon noise is 2.07×10^{-17} W/$\sqrt{\text{Hz}}$. (color version online)

5 Outlook

We have demonstrated our design goal of photon-noise dominated 40 GHz devices for use in the first BA receiver. Now we are half-way through the fabrication of 40 GHz tiles, and the rest are expected to come in the following month. The design of 30 GHz detector tiles has been finished, with similar considerations from the 40 GHz development process. Experience and knowledge accumulated in 40 GHz gives us confidence in a successful 30 GHz development as well. The first 30 GHz tile is currently under fabrication and is expected to be tested by Fall 2019. We expect that after 3 full years of observations, all four BICEP Array cameras will measure primordial gravitational waves to a precision (r) between 0.002 and 0.004, depending on foreground complexity and the degree of lensing removal.

References

1. Bicep/Keck Collaboration *Phys. Rev. Lett.* **121**, 22, (2018), DOI: 10.1103/PhysRevLett.121.221301
2. H. Hui, et al, *Proc. SPIE* **10708**, id. 1070807, (2018), DOI: 10.1117/12.2311725
3. M. Crumrine, et al, *Proc. SPIE* **10708**, id. 107082D, (2018), DOI: 10.1117/12.2312829
4. BICEP2 and Keck Array Collaboration, SPIDER Collaboration *ApJ* **812**, 176, (2015), DOI: 10.1088/0004-637X/812/2/176
5. A. Schillaci, et al, *J. Low Temp. Phys.*, This Special Issue (2019)
6. A. Soliman, et al, *J. Low Temp. Phys.*, This Special Issue (2019)